Discrete soliton ratchets driven by biharmonic fields

Yaroslav Zolotaryuk[1] and Mario Salerno[2]

[1]*Bogolyubov Institute for Theoretical Physics, National Academy of Sciences of Ukraine, Kyiv 03143, Ukraine*
[2]*Dipartamento di Fisica "E. R. Caianiello" and Consorzio Nazionale Interuniversitario per le Scienze Fisiche della Materia (CNISM),*
Universitá di Salerno, I-84081 Baronissi, Salerno, Italy
(Received 20 January 2006; published 23 June 2006)

Directed motion of topological solitons (kinks or antikinks) in the damped and ac-driven discrete sine-Gordon system is investigated. We show that if the driving field breaks certain time-space symmetries, the soliton can perform unidirectional motion. The phenomenon resembles the well known effects of *ratchet* transport and nonlinear harmonic mixing. Direction of the motion and its velocity depends on the shape of the ac drive. Necessary conditions for the occurrence of the effect are formulated. In comparison with the previously studied continuum case, the discrete case shows a number of new features: nonzero depinning threshold for the driving amplitude, locking to the rational fractions of the driving frequency, and diffusive ratchet motion in the case of weak intersite coupling.

I. INTRODUCTION

Transport phenomena induced by the interplay between nonequilibrium fluctuations, symmetry breaking, and nonlinearity, have recently attracted a great deal of interest. In particular, point particle ratchets described by ordinary differential equations have been largely investigated due to their relevance in several fields, including molecular motors and Josephson junctions (see reviews [1,2]). In simple terms, the point particle ratchets appear as the unidirectional motion of a damped and driven particle, which is achieved under the influence of only stochastic and deterministic forces of zero average, independently on initial conditions. The phenomenon was ascribed to the breaking of the symmetries connecting orbits with opposite velocities in the phase space [3–5] and to the phase locking of the particle dynamics to the external driver [6–8].

Ratchet phenomena in infinite-dimensional systems described by nonlinear partial differential equations of soliton type have also been investigated. This has been done for both spatially asymmetric potentials with temporarily symmetric ac fields [9,10] and for symmetric potentials with temporarily asymmetric ac fields [11–14]. In both cases, the ratchet effect appears as a unidirectional motion of the soliton, which resembles the drift dynamics observed for point particle ratchets; from here the name of *soliton ratchets* [10]. Soliton ratchets induced by asymmetrical external fields have been implemented experimentally in long Josephson junctions [15] by means of *nonlinear harmonic mixings*. This approach has been shown to be effective also in other physical contexts [16] (for a detailed list of references see the review paper [2]). The existence of soliton ratchets in long Josephson junctions was also experimentally demonstrated by using asymmetric magnetic fields [17] and spatially asymmetric currents [18]. From the theoretical point of view, symmetry breaking conditions to generate soliton ratchets were discussed in Ref. [12]. The mechanism underlying soliton ratchets was proposed in Ref. [10] for the case of a perturbed asymmetric double sine-Gordon equation driven by a symmetric ac driver and extended in Ref. [11] to the

case of the damped sine-Gordon (SG) equation with asymmetric ac fields. In both cases, the phenomenon was ascribed to the existence of an internal oscillation on the kink profile which, in the presence of damping, couples to the translational mode of the kink and produces transport. The internal vibration was shown to be spatially asymmetric, thus giving directionality to the motion, and phase locked to the external force. This mechanism, also known as the *internal mode mechanism*, has been confirmed for a number of systems such as the asymmetric double sine-Gordon equation with symmetric driver [10,19] and the SG system with temporal asymmetric forces [11,20,21].

In contrast to the continuous case, however, discrete soliton ratchets have been scarcely investigated (some work on spatially asymmetric discrete soliton ratchets has been done in Refs. [22–25]). In this case, one can expect that the presence of the Peierls-Nabarro barrier can strongly influence the transport of discrete solitons. It is therefore of interest to investigate the conditions under which the discrete soliton ratchets can exist. The present paper is just devoted to this investigation. More precisely, we study the ratchet dynamics induced by temporarily asymmetric forces of zero mean on topological solitons (kinks and antikinks) of the discrete sine-Gordon (DSG) system. This equation models a number of physical systems such as arrays of Josephson junctions, crystal dislocations, or charge-density waves (see [26,27]). In particular, we investigate the conditions for the occurrence of soliton ratchets and study the dependence of the average soliton velocity on the system parameters. A comparison with the results derived for continuous soliton ratchets in Ref. [11] is also provided.

From our study it emerges that discrete soliton ratchets are much more complicated than their continuum counterpart. In particular, the mean velocity of the kink in most cases appears to be a piecewise function of the parameters which resembles a devil's staircase. We find that kink transport becomes very effective on the corresponding orbits (limit cycles) which are phase locked to the external driver. Transport is possible also in the presence of more complicated dynamics such as chaotic and intermittency orbits, especially when the system becomes very discrete (this is

achieved when the coupling constant is very small). In these cases, however, the kink transport is not very efficient since the drift velocity is rather small. Except for the very discrete case, dominated by the pinning of the kink to the lattice, we find that the internal mode mechanism remains valid also in the DSG ratchet in all cases in which the transport is observed.

We remark that the soliton ratchets induced by temporarily asymmetric fields may be an effective way to control the transport properties of a large variety of continuous and discrete systems. From the experimental point of view, indeed, it is much easier to produce ratchets by means of asymmetric fields than by breaking the internal spatial symmetry of the system [28], since in the former case no structural changes of the system are required.

The paper is organized as follows. In Sec. II, we present the model. In Sec. III we derive the necessary condition for the directed kink motion in terms of a simple symmetry analysis, which is based on a point particle description of the kink dynamics. In Sec. IV we describe the desymmetrization mechanism and confirm the results by means of numerical simulations. In Sec. V, we study the dependence of discrete kink ratchets on the system parameters. In particular, we investigate the dependence of the mean velocity of the kink on the amplitude, phase, and frequency of the ac driver as well as on the damping and the coupling constant. Moreover, the validity of the internal mode mechanism in the discrete case is discussed. In Sec. VI, we consider the soliton ratchet in a finite lattice and discuss possible applications of the phenomenon to arrays of small Josephson junctions. Finally, in Sec. VII, we summarize the main conclusions of the paper.

II. THE MODEL

The ac driven and damped discrete sine-Gordon (DSG) equation is introduced in a dimensionless form as follows

$$\ddot{u}_n - \kappa \Delta u_n + \sin u_n + \alpha \dot{u}_n + E(t) = 0, \quad n = 1, 2, \ldots, N. \tag{1}$$

Here u_n is the displacement of the nth particle from its equilibrium position, $\Delta u_n \equiv u_{n+1} - 2u_n + u_{n-1}$ is the discrete Laplacian, κ is the coupling constant measuring the discreteness of the lattice, α is the damping coefficient, and $E(t)$ is an external driving field. In the following we assume $E(t)$ to be of the form

$$E(t) = E_1 \cos(\omega t) + E_2 \cos(m\omega t + \theta), \tag{2}$$

where m is an integer even number. Notice that the superposition of two harmonics makes the periodic force to be asymmetric in time for almost all values of θ, a feature which can be used to break the temporal symmetry of the system (see below). In this context, it is of interest to investigate the condition under which a driving force of zero mean of type (2) can induce kink's unidirectional motion similar to the one observed in the continuum SG case [11]. In this regard, we remark that in the lower approximation, a discrete kink of the form $u_n(t) = 4 \arctan\{\exp[n - X(t)]\}$, can be viewed as a single particle [27] and its dynamics is described in terms of col-

lective coordinates: the center of mass $X(t)$ and the kink velocity $\dot{X}(t)$. In this approach, the effective point-particle equation of the motion becomes

$$\ddot{X} + \alpha \dot{X} + V'_{PN}(X) + \widetilde{E}(t) = 0, \tag{3}$$

where $V_{PN}(X) = V_{PN}(X+1)$, $V'_{PN}(X) \sim \sin 2\pi X$ is the Peierls-Nabarro (PN) potential accounting for the discreteness of the lattice and $\widetilde{E}(t) \sim E(t)$ is the effective driving field of the kink [we assume $\widetilde{E}(t)$ to be proportional to $E(t)$]. An important parameter of the problem is the frequency of kink oscillations in the bottom of the PN potential (the PN frequency), which can be written as [33]

$$\omega_{PN} = \sqrt{2\pi\alpha_0 \kappa^{3/2}} \exp(-\pi^2 \sqrt{\kappa}/2), \quad \alpha_0 \simeq 30\pi. \tag{4}$$

Within this approximation, the unidirectional motion of the kink corresponds to a limit cycle of Eq. (3), which is phase locked to the frequency of the external driver. On this orbit, the average kink velocity is expressed as

$$\langle v \rangle = \langle \dot{X}(t) \rangle = \frac{k}{l} \frac{\omega}{2\pi}, \tag{5}$$

with k and l being integer numbers. Notice that in this resonant regime, the kink travels k sites during the time $lT = 2\pi l/\omega$, so that, except for a shift in space, its profile is completely reproduced after this time interval (in the pendulum analogy, this orbit corresponds to k full rotations of the pendulum during l periods of the external drive). In the following, we will refer to the phase locked dynamics also as to *resonances*.

III. SYMMETRY PROPERTIES AND CONDITIONS FOR TRANSPORT

In analogy with the continuous SG case[11,12], one can expect that the directed kink motion arises when all the symmetries of Eq. (3), which relate kink solutions with opposite velocities, are broken. Qualitative conditions for the occurrence of this directed motion can be obtained from the analysis of the symmetry properties of Eq. (3). In this approach, the many-particle problem is reduced to the one-particle ratchet studied before [3,4] [we neglect oscillations of the discrete kink profile (to be discussed later) which also contribute to the phenomenon]. Our analysis is based on the simple observation that the sign of the soliton velocity $\dot{X}(t)$ can be changed by means of the following symmetry operations:

$$\hat{\mathbf{D}}_{\mathcal{X}}: t \rightarrow t + T/2, \quad X \rightarrow -X, \tag{6}$$

$$\hat{\mathbf{D}}_{\mathcal{T}}: X \rightarrow X + X_0, \quad t \rightarrow -t + 2t_0, \tag{7}$$

where $\hat{\mathbf{D}}_{\mathcal{X}}$ denotes a shift in time followed by a reflection is space and $\hat{\mathbf{D}}_{\mathcal{T}}$ is a shift in space followed by a reflection in time (here t_0 is a constant and X_0 is either an integer or a half integer). Notice that Eq. (3) is always invariant under the symmetry $\hat{\mathbf{D}}_{\mathcal{X}}$ provided the external driver satisfies

$$E(t) = -E(t + T/2). \quad (8)$$

Notice that $V_{PN}(-X) = V_{PN}(X)$ is always satisfied because the sine-Gordon potential is symmetric. In the zero damping limit ($\alpha \to 0$), Eq. (3) becomes invariant also under the symmetry $\hat{\mathbf{D}}_T$ with $X_0 = 1$, provided the external driver satisfies the condition

$$E(t + t_0) = E(-t + t_0), \quad (9)$$

with t_0 being a constant, which depends on the shape of $E(t)$. In the overdamped limit ($\alpha \to \infty$), Eq. (3) can be rewritten as $\dot{X} + V'_{PN}(X) + \widetilde{E}(t) = 0$ from which one can see that it becomes invariant under the symmetry $\hat{\mathbf{D}}_T$ with $X_0 = 1/2$, provided the external driver satisfies the condition

$$E(t + t_0) = -E(-t + t_0). \quad (10)$$

It should be remarked here that $V'_{PN}(X) = -V'_{PN}(X + 1/2)$ is always satisfied since for the DSG equation we have that $V'_{PN}(X) \sim \sin 2\pi X$. From the above symmetry properties it follows that one can break all symmetries relating orbits with opposite velocities by properly choosing the driving force $E(t)$. Thus, for the general case $\alpha \neq 0$, we have only the symmetry $\hat{\mathbf{D}}_{\mathcal{X}}$ for Eq. (3). This symmetry can be broken by choosing any function $E(t)$ which violates Eq. (8). In the zero damping limit ($\alpha \to 0$), we have, besides $\hat{\mathbf{D}}_{\mathcal{X}}$, also the symmetry $\hat{\mathbf{D}}_T$ with $X_0 = 1$. In this case, one must choose a driving field $E(t)$ which violates both Eqs. (8) and (9). Similarly, in the overdamped limit ($\alpha \to \infty$), a function $E(t)$ which violates both Eqs. (8) and (10) should be chosen.

From these considerations it follows that a simple sinusoidal driver cannot support the kink transport in the lattice, since Eqs. (6)–(10) in this case are always satisfied. For a biharmonic driver of the type (2), however, we have that Eq. (8) is violated for any θ (if m is even), so that the kink transport should become possible.

From these arguments it is also clear that an external periodic driver of zero mean, which consists of the superposition of only the first two harmonics, is the simplest driver that can be used to induce the soliton ratchets in the DSG system.

IV. NUMERICAL STUDY OF TRANSPORT VS SYMMETRIES

To verify the validity of the previous analysis and to check the desymmetrization of the orbits as a function of the driver parameters E_1, E_2, and θ, we recourse to direct numerical integration of Eqs. (1). In order to be sure that the system explores the whole phase space and that the phenomenon does not depend on initial conditions, we perform the first step: simulations in the presence of white noise. White noise has been included by adding in the right-hand side of Eqs. (1) a stochastic term $\xi_n(t)$ of zero mean, $\langle \xi_n(t) \rangle = 0$, and with the autocorrelation function $\langle \xi_n(t) \xi_m(t') \rangle = 2\alpha D \delta_{mn} \delta(t - t')$. The resulting Langevin equations have been integrated numerically by using the fourth-order Runge-Kutta method, adopting either free ends or periodic boundary conditions:
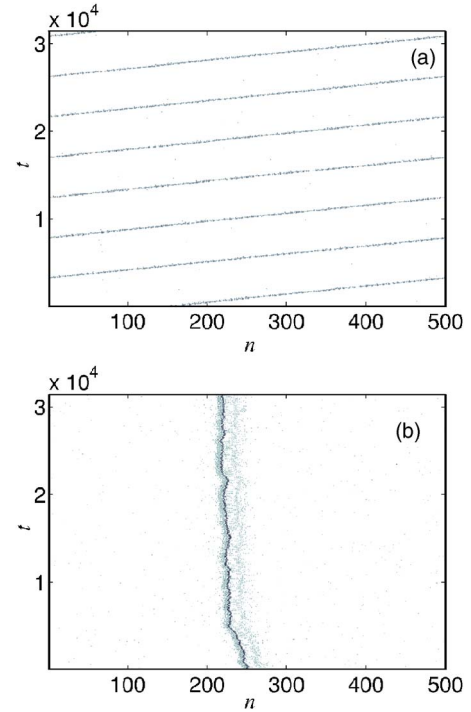

FIG. 1. (Color online) Contour plot of the temporal evolution of the particle velocities $\dot{u}_n(t)$ for (a) $E_1 = 0.3$, $E_2 = 0.15$ and (b) $E_1 = 0.45$, $E_2 = 0$. Other parameters are: $\kappa = 1$, $\alpha = 0.05$, $\omega = 0.1$, $\theta = 2$, $D = 0.002$, $N = 500$. Periodic boundary conditions have been applied.

$u_{n+N}(t) = u_n(t) \pm 2\pi$ (positive and negative signs refer to kinks and antikinks, respectively).

Figure 1 illustrates the dynamics of a kink of the damped DSG equation under the influence of noise, driven by a biharmonic driver (2) with $m = 2$ [panel (a)], and by a single harmonic driver [panel (b)]. We see that while the single harmonic driver is unable to produce directed motion, the biharmonic driver is quite effective to produce the kink transport. From this figure, one can also observe that there is only one attractor corresponding to the unidirectional motion of the kink. Further investigations (see below and Sec. V) show that this is true in almost all cases, except for very narrow intervals in the parameter space where two attractors can coexist.

This fact makes possible to investigate Eqs. (1) in the absence of noise without averaging over the initial conditions. In Fig. 2 we plot the time average kink velocity $\langle v \rangle$ as a function of the phase difference θ in the case of a biharmonic driver with $m = 2$. In contrast to the continuous case for which $\langle v \rangle$ was shown to have a sinusoidal dependence on θ [11,13], in the discrete case, we find a complicated piecewise dependence $\langle v \rangle(\theta)$, which resembles a sinusoidal function only slightly. This is due to the fact that in most cases the dynamics is phase locked to the external driver and the kink velocity is given by Eq. (5).

Notice that for a weak damping [see panel (a) of Fig. 2] several resonances ($k = l = \pm 1$, $k = \pm 2$, $l = 1$) are clearly visible, while for a strong damping [panel (c)], the kink becomes pinned to the lattice for large intervals of θ (depinning of the kink would require stronger fields). From Figs.
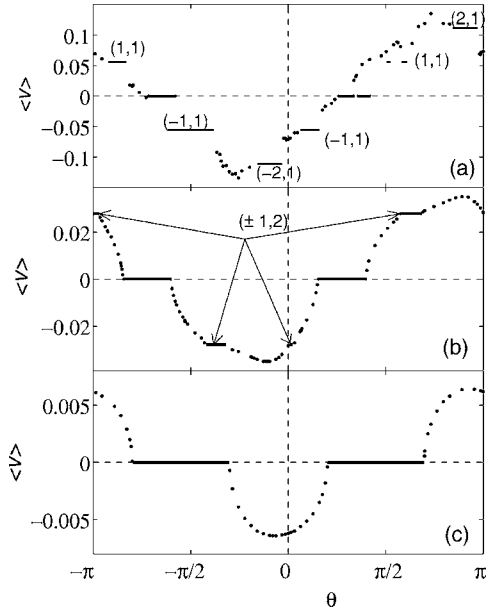
FIG. 2. Dependence of the average kink velocity on the phase difference θ for $E_1=E_2=0.2$, $\alpha=0.05$ (a), $\alpha=0.2$ (b) and $\alpha=0.5$ (c). Other parameters are: $\kappa=1$, $\omega=0.35$. Corresponding pairs of rotation numbers (k,l) are given nearby the most pronounced resonances. Dashed lines mark the coordinate axes.

2(a)–2(c) a qualitative understanding of the symmetries to break, in order to achieve unidirectional motion, can be obtained. In particular, one can see that close to the underdamped limit ($\alpha=0.05$), the mean velocity becomes zero in the intervals $\theta \in [-2.26,-1.81]$, $\theta \in [0.80,1.06]$, and $\theta \in [1.11,1.33]$ [see Fig. 2(a)]. For larger values of the damping constant [see Fig. 2(b)], we have $\langle v \rangle=0$ in the intervals $\theta \in [-2.66,-1.88]$ and $\theta \in [0.48,1.26]$, while for $\alpha=0.5$, the kink stays pinned for $\theta \in [-2.5,-0.95]$ and $\theta \in [0.64,2.19]$. By increasing α, the extremal values of $\langle v \rangle$ shift to 0 or $\pm\pi$ with the growth of α. Moreover, the length of the intervals in θ where $\langle v \rangle=0$ increases, while the average kink velocity decreases as α increases. This behavior is an obvious consequence of the slowing down effect of the damping on the kink motion. In the overdamped limit $\alpha \to \infty$, the intervals become centered around the points $\theta=\pm\pi/2$ for which $E(t)=E_1 \cos \omega t+E_2 \cos(2\omega t+\pi/2)=-E(\pi/\omega-t)$ and thus the symmetry (6) is satisfied. Instead, in the underdamped case ($\alpha \to 0$), the centers of these intervals gradually shift to the positions $\theta=0,\pm\pi$ for which $E(t)=E(-t)$ and the symmetry (7) is satisfied.

We recall that in the continuum case [11], the functional dependencies obtained in the underdamped and overdamped limits were found to be $\langle v \rangle \sim \sin \theta$ and $\langle v \rangle \sim \cos \theta$, respectively. Thus, the transition from one limit to another in the discrete case is similar to the continuous case in the sense that the directed soliton motion disappears in correspondence with values of θ for which the respective symmetry is restored. In the discrete case, however, the soliton velocity is zero not only for those values of θ which restore the symmetries (6) and (7), but also for some finite interval around these values.
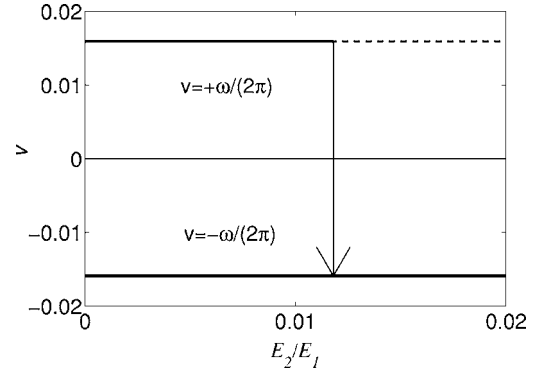

FIG. 3. Velocities of two kinks, running into the opposite directions at $\alpha=0.05$, $\omega=0.1$, $E_1=0.21$, $\theta=0$ as a function of E_2/E_1. Dashed line denotes that the given solution is no longer stable.

In the case of odd values of m, the condition (8) is satisfied for any value of θ if $E_2 \neq 0$. We have indeed that $E(t+T/2)=E_1 \cos(\omega t+\pi)+E_2 \cos(m\omega t+m\pi+\theta)=-E(t)$ and therefore the symmetry $\hat{\mathbf{D}}_\chi$ is always valid. This observation implies that there should be no kink transport in the system, a result which is indeed confirmed by direct numerical simulations of the full system with $m=3$, both in the presence and in the absence of noise. Also, in analogy with the continuous case, we find that for the same parameter values the discrete antikink ratchets always move in the direction opposite to the kink motion.

The emergence of the directed kink motion can also be seen as a consequence of the desymmetrization of the basins of attraction of the two limit cycles corresponding to kinks moving with opposite velocities (for single particle ratchets, the desymmetrization of the orbits has been shown in Refs. [3,7]).

As soon as the symmetry is broken (by switching on the field E_2), one of the basins of attraction begins to shrink and eventually disappears as E_2 increases. As a result, only the limit cycles which correspond to motion in one direction survive, as one can see from Fig. 3.

In particular, for the parameters given in this figure, we find that the attractor corresponding to the limit cycle with rotation numbers $k=1,l=1$ disappears at $E_2/E_1=0.0118$, i.e., already for a rather weak asymmetry of the field ($E_2 \ll E_1$).

V. DEPENDENCE OF THE PHENOMENON ON SYSTEM PARAMETERS

In this section, we investigate the dependence of kink dynamics on the system parameters such as amplitude and frequency of the internal driver, interaction and damping constants, and also investigate the internal mode mechanism of the kink transport.

A. Dependence on the driving amplitude

For continuous ratchets it was shown previously [11] that the average kink velocity is proportional to $E_1^2 E_2$, so that, provided the respective symmetries are broken, the directed motion can occur for arbitrary small values of the driving
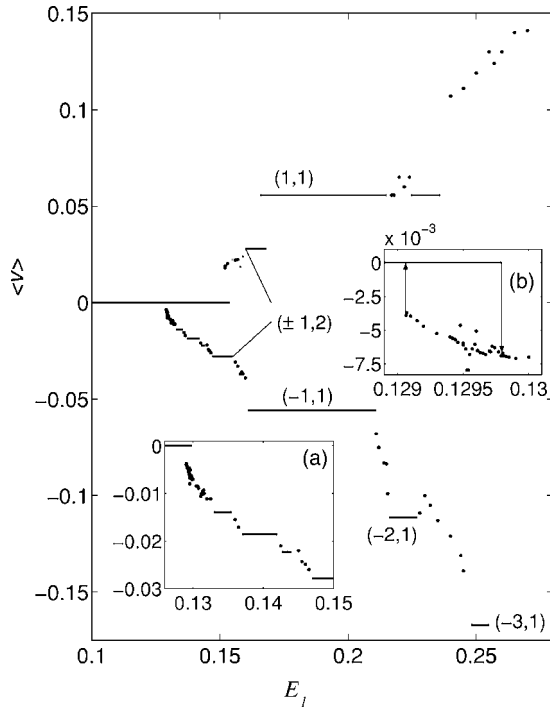
FIG. 4. Dependence of the average kink velocity on the amplitude of the driver $E_1=E_2$ for $\theta=-0.5$ (decreasing dependence) and $\theta=2$ (increasing dependence). Other parameters are: $\alpha=0.1$, $\kappa=1$, $\omega=0.35$. Numbers in brackets show the respective pair of rotation numbers (k,l). Insets show more details for case $\theta=-0.5$.

amplitudes. For the DSG equation, the dependence of the average kink velocity on the driver amplitudes is depicted in Fig. 4 from which one can see that the kink velocity is not a smooth monotonic function of $E_{1,2}$, but a piecewise function with plateaus of different lengths, resembling a "devil's staircase" [the same as in Fig. 2(a) but monotonic]. The plateau values of the kink velocities are given by Eq. (5) and corre-

spond to dynamical regimes, which are limit cycles with rotation numbers (k,l) phase locked to the driver. Notice that the largest resonant step ($\langle v \rangle=0.0557$) is achieved at the rotation numbers corresponding to the main resonance ($k=\pm1,l=1$). One can easily observe the smaller resonant steps with $k=\pm2,l=1$ and $k=\pm1,l=2$, for which the kink velocities equal $\langle v \rangle=0.1114$ and $\langle v \rangle=0.02785$, respectively. Higher order resonances can also be identified, but they are not well visible in the figure.

A main feature of the discrete case is the existence of a threshold in the driver amplitude (depinning threshold) above which the transport occurs. For driving amplitudes below the threshold the kink remains pinned to the lattice and its center of mass

$$X_c = \frac{\sum_{n=1}^{N} n(u_{n+1} - u_{n-1})}{2(u_N - u_1)} \qquad (11)$$

oscillates around a lattice site. This is shown in Fig. 5 where X_c is plotted as a function of time for different values of the driving amplitude. Panel (a) of this figure refers to the case of driving amplitudes below threshold while panels (b)–(e) refer to the case of amplitudes above threshold at which the standing kink becomes unstable and the directed motion starts. Notice that for higher amplitudes the kink motion can be either chaotic with an intermittent behavior [see panels (b) and (c)] or phase locked to the external driver with rotation numbers $k=1,l=5$ [see panels (d) and (e)]. Also notice that in this last case the kink travels over a fixed number of sites during each period T in agreement with Eq. (5). By further increasing E_1, we observe that the kink dynamics may start to switch between periodic (or quasiperiodic) regime and intermittency. Similar chaotic transitions in the case of a single harmonic driver were reported in Refs. [26,31]. In the intermittency regime, the kink dynamics switches in an unpredictable manner between two attracting limit cycles [see pan-
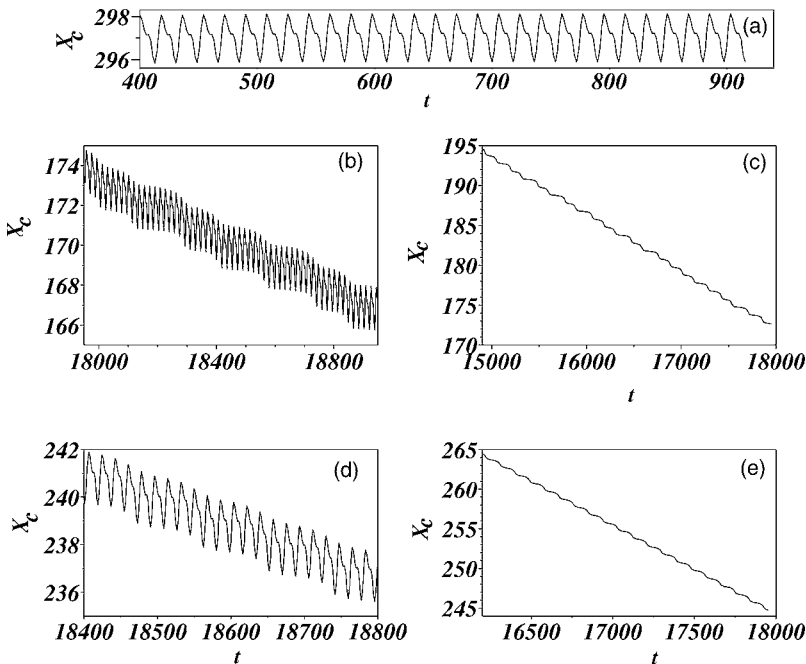

FIG. 5. Coordinate of the kink center X_c as a function of time for different values of the driving amplitude $E_1=E_2=0.129$ (a); 0.129 81 (b,c) and 0.1309 (d,e). In panels (c) and (e), $X_c(t)$ has been plotted after each oscillation period T (see text for details). Other parameters are: $\alpha=0.1$, $\omega=0.35$, $\kappa=1$, $\theta=-0.5$.

els (b) and (c) of Fig. 5]. In this case, the kink dwells some time interval on a certain site, pinned by the corresponding minimum of the PN barrier, before jumping to the next site. From panel (b) one can also see that the dwelling time is not rationally related to the driving period T and changes randomly from jump to jump. Thus in the intermittent regime the kink does not travel the same number of sites during an integer number of periods of $E(t)$ and the global dynamics is chaotic.

The same behavior is seen in panel (c) of Fig. 5 for a larger time scale. Note that the intermittency behavior occurs not only around the depinning threshold, but also for larger values of the driving amplitude. Also notice, from the inset (b) of Fig. 4, that the depinning threshold has an hysteretic behavior. In this regard, we remark that the numerical investigation has been performed by increasing the driving amplitude in small steps, taking the final state for a given step as an initial condition of the next one. When the pinned state loses stability, the system finds itself on a chaotic attractor, which corresponds to the directed motion. By increasing further E_1 we obtain larger values of the kink velocity, while if we move backwards, we observe that two attractors can coexist—one of them corresponding to a pinned kink oscillating around its center of mass, and the other to a kink performing ratchet dynamics. If E_1 is further decreasing, the moving state loses stability and the system jumps back to the pinned state. The width of the hysteresis (interval between two bifurcations) appears to be rather small, i.e., 0.129 065 $< E_1 <$ 0.12979. Similar hysteretic phenomena also appear at larger values of the driver amplitudes. For example, one can find that in the interval $0.1660 < E_1 < 0.1678$, two limit cycles with $k=1, l=2$ and $k=1, l=1$ coexist. Coexistence of attractors and existence of hysteresis was observed also in point particle ratchets [7].

A more detailed numerical investigation of the $\langle v \rangle (E_1)$ dependence shows that there are gaps of the value $\langle v \rangle$ in the observed devil's staircase and these gaps depend on θ. As the $\langle v \rangle (E_1)$ dependence becomes steeper, less phase locked states are found. In particular for the case $\theta=2$, one can see that in the transition from the $k=1, l=2$ to the $k=1, l=1$ state, all steps that correspond to the intermediate rational values of k and l are missing.

B. Dependence on the driving frequency

The dependence of the mean kink velocity on the driver frequency was investigated in Ref. [11] for the continuous SG model. In this case, it was shown that the average velocity depends on the driving frequency as $\langle v \rangle \sim \sin[\theta - \theta_0(\omega; \alpha)]/\omega^3$, where $\tan \theta_0(\omega; \alpha) = [\alpha/(2\omega)][3 + (\alpha/\omega)^2]$. This fact implies that $\max_{\theta \in [0, 2\pi[} \langle v \rangle$ decays with the growth of ω. For a fixed value of θ, however, this dependence is defined by the mutual relations between ω and α, so that $\langle v \rangle$ can experience oscillations and sign reversals before tending to zero either in a decreasing or in increasing way. Similar behavior is expected also for the DSG equation, although in this case, the problem is complicated by the presence of the Peierls-Nabarro (PN) frequency ω_{PN} in Eq. (3). In analogy with Fig. 2, one can expect the dependence $\langle v \rangle (\omega)$ to be also
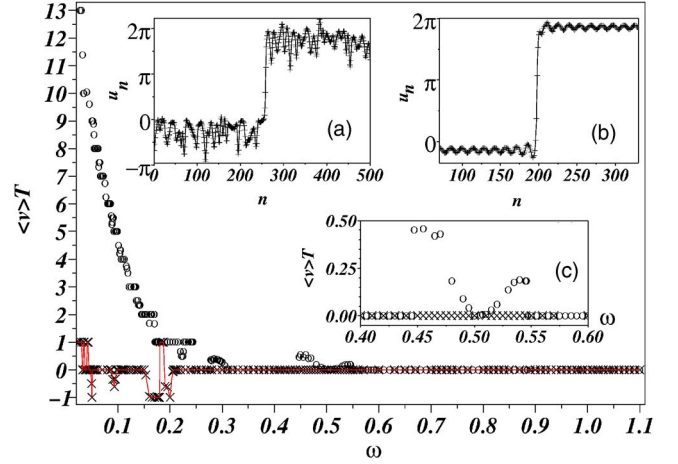

FIG. 6. (Color online) Dependence of the normalized kink velocity $\langle v \rangle T$ on the driving frequency for $E_1 = E_2 = 0.1$, $\theta = 2$, $\alpha = 0.05$ ($\circ$) and $E_1 = E_2 = 0.02$, $\theta = 1.5$, $\alpha = 0.15$ ($\times$). In both cases $\kappa = 1$. The insets (a) and (b) show the kink profile for the first set of parameters when $\omega = 0.45$ and $\omega = 0.507$, respectively. Inset (c) shows more detailed behavior around $\omega = 0.5$. The connecting lines in all cases have been used as guides to an eye.

a piecewise function with a devil's staircase character.

In Fig. 6, we depict the kink velocity, normalized to the driving frequency ($\langle v \rangle T = 2\pi v / \omega$) as a function of ω for two values of the damping constant (notice that for phase locked dynamics, $\langle v \rangle T$ coincides with the ratio of rotation numbers k/l). One can see that the dynamics is characterized by a series of resonances, the most pronounced one being at the main frequency ($k=1, l=1$). We also observe that the resonances with $k > l$ are less pronounced and the subharmonic resonances with $k < l$ are practically not visible in the figure. The case of small damping and larger driver amplitude (depicted in the figure by circles) is characterized by an almost monotonic decay, while in the opposite case (larger damping and smaller driving amplitude), there are wide pinned regions and some peak around the value of ω_{PN} [notice from Eq. (4) that $\omega_{PN} \simeq 0.17$ for $\kappa = 1$].

In both the cases we find that, except for the resonances $\omega \approx \omega_L$ and $2\omega \approx \omega_L$, where ω_L is the frequency of linear waves

$$\omega_L^2(q) = 2\kappa(1 - \cos q) + 1, \qquad (12)$$

the kink transport becomes effective mainly at low frequencies $\omega \ll \omega_L$ and disappears for driving frequencies $\omega > \omega_L$. Also, from Fig. 6 one can see that the kinks become pinned to the lattice for values of ω significantly smaller than ω_L. At the resonances $\omega \approx \omega_L$ and $2\omega \approx \omega_L$, we observe that the kink dynamics become coupled to linear waves in the system (plasmons in the case of array of Josephson junctions). Insets (a) and (b) of Fig. 6 show the profiles of the kink solution in these resonant cases, while inset (c) shows details of the $\langle v \rangle$ dependence in the neighborhood of the second resonance. The coupling of the kink motion with linear waves occurs in the interval $0.447 < \omega < 0.517$. At the beginning of this interval, the kink displays a chaotic tail as shown in Fig. 6(a). As

frequency increases, the chaotic tail becomes more and more regular. This is shown in inset (b) of the figure, from which one can see that at $\omega=0.507$ the oscillating tail is almost monochromatic. At $\omega=0.517$ the oscillating tail turns into a localized oscillating mode which decays at infinity. A further increase of the driving frequency causes the decay of the width of the mode.

A similar scenario occurs also at $\omega \approx \omega_L$, but in this case the kink velocity is much smaller and practically not visible in Fig. 6. Notice that in the frequency interval $0.895 < \omega < 1.05$, the kink becomes again coupled to linear modes and displays a chaotic tail, which becomes more regular as ω further increases. At the beginning of this window, the dynamics in the tails are strongly chaotic and they are accompanied by the formation of large-amplitude localized excitations (breathers).

By reducing the driving amplitude, the frequency windows, in which the coupling with linear waves occurs, decrease. We find that for $E_1=E_2=0.04$, the first coupling window occurs at $0.480 < \omega < 0.495$ and the second one at $0.955 < \omega < 0.994$. In this case, no chaotic dressing of the kink is observed [the coupling occurs with very few (or single) linear modes and the kink looks very similar to that in Fig. 6(b)]. For the driving amplitude $E_1=E_2=0.01$, the coupling with linear waves does not take place at all, and around the resonant frequencies ω_L and $\omega_L/2$, the kink remains pinned to the lattice. As the driving amplitude increases, beyond a certain threshold chaotic oscillations can completely destroy the kink. From these results, we conclude that the coupling of the kink dynamics with linear waves depends very much on the amplitude of the external field and this effect is nonlinear in E_1. Near the resonances with linear modes, the kink dynamics become more chaotic (diffusive), resembling the one of a Brownian particle (the kink makes many random jumps backward and forward and the unidirectional motion can be seen only at a large time scale).

C. Dependence on the coupling constant

In this section, we investigate the dependence of the ratchet phenomenon on the interaction constant κ and the conditions to sustain mobile kinks in the system. As well known [34], the discreteness usually prevents free topological soliton propagation. In our model, the discreteness of the system is characterized by the interaction constant κ, with $\kappa \to \infty$ corresponding to the continuum limit. In Fig. 7, we depict the temporal evolution of the kink center of mass X_c for two values of the coupling constant $\kappa=0.5$ [panel (a)] and $\kappa=0.25$ [panel (b)]. From this figure, we conclude that the unidirectional motion exists also for small values of κ with dynamics which is chaotic rather than phase locked (see insets of the figure).

Chaotic motion, leading to transport is found to be either of the intermittent type [curve 4 of panel (a)] or diffusive type [curves 1–3 of panel (a)]. The intermittent regime is more often observed for $\kappa \gtrsim 1$ and the behavior is the same as described in the previous section, i.e., the kink oscillates in the minima of the PN potential until it jumps to the adjacent site [see lower inset of panel (a)]. The motion is char-
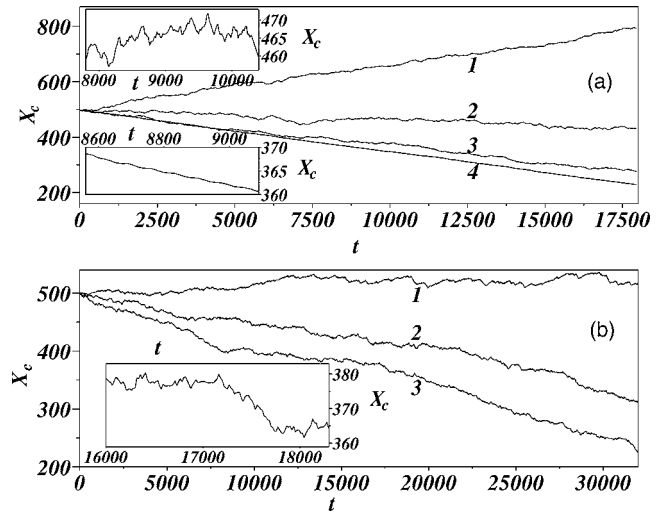

FIG. 7. Time evolution of the position of the kink center for: (a) $\kappa=0.5$; $E_1=E_2=0.21$ (curve 1), 0.19 (curve 2), 0.17 (curve 3), 0.11 (curve 4), and (b) $\kappa=0.25$; $E_1=E_2=0.14$ (curve 1), 0.24 (curve 2), 0.22 (curve 3). Other parameters are: $\theta=1.5$, $\alpha=0.1$, $\omega=0.35$. The upper inset of panel (a) corresponds to details of the case $E_1=E_2=0.19$ and the lower inset corresponds to the case $E_1=E_2=0.11$. The inset of panel (b) corresponds to the case $E_1=E_2=0.22$. In all figures, the data have been plotted with the interval $T=2\pi/\omega$.

acterized by the fact that the jumps of the kink occur randomly in time, but always in the same direction. For $\kappa \lesssim 1$ the diffusive motion is the most typical scenario. In this case, the kink jumps randomly forward and backward [see upper inset of panel (a) and inset of panel (b)], but on average the motion remains unidirectional. A decrease of the coupling constant makes the dynamics even more diffusive in the sense that the forward and backward jumps become of larger amplitude with a consequent decrease of the average velocity.

In the left panel of Fig. 8 the diagram of possible dynamical regimes in the plane (κ, E_1) is shown. We observe that by changing the coupling constant κ, one can pass from regular (phase locked) dynamics to chaos. The regular dynamics are dominant for $\kappa > 1$ and when κ is decreased, the windows of chaotic motion appear. By further decreasing κ, the number of chaotic windows increases and the chaotic motion becomes dominant. At $\kappa=0.25$, almost no regular dynamics exist. Notice that the diagram in Fig. 8 does not show the complete picture and the details of transitions to different dynamical regimes because in order to limit the computation time, we have used in the numerical calculations the step of 0.01 in the amplitude of the driving field $E_1=E_2$ and a coarse step of 0.25 in κ. We find that for driving amplitudes $E_1=E_2 \gtrsim 0.3$, the chaotic dynamics of the *whole lattice* destroy kink solutions.

In the right panel of Fig. 8, we show the dependence of the average kink velocity on the driving amplitude $E_1=E_2$ for different values of the coupling constant κ. We observe that already for $\kappa=2$, the curve is very smooth (except for the small resonant steps $k=3, l=1$ and $k=3, l=2$) and the behavior becomes very similar to that reported for the continuous limit ($\langle v \rangle \sim E_1^2 E_2$) [11]. By increasing the driving

FIG. 8. (Color online) *Left panel.* Diagram that demonstrates main regimes of the kink ratchet motion for different values of the coupling constant κ and the driving amplitude $E_1=E_2$ (other parameters are: $\theta=1.5$, $\alpha=0.1$, and $\omega=0.35$). In the diagram $\circ$ stands for the regime when kink is pinned ($\langle v \rangle=0$), $\oplus$ stands for the periodic or quasiperiodic ratchet motion, $\times$ stands for the chaotic regime, and $\blacklozenge$ corresponds to the case when kink solutions do not exist. *Right panel.* Dependence of the average kink velocity on the driving amplitude $E_1=E_2$ for different values of the coupling constant $\kappa=0.5$ ($\triangle$), $\kappa=0.75$ ($\times$), $\kappa=1$ ($\diamond$), $\kappa=1.5$ ($\blacklozenge$), and $\kappa=2$ ($\circ$). Other parameters are as in the left panel. The insets show dependence of the average velocity on the phase difference θ. Inset (a) corresponds to $\kappa=0.75$, $E_1=E_2=0.19$ ($\circ$) and $E_1=E_2=0.25$ ($\blacklozenge$), inset (b) corresponds to $\kappa=0.5$, $E_1=E_2=0.22$ ($\oplus$). The connecting lines are drawn as guides to an eye.

amplitudes $E_{1,2}$, the dependence becomes nonmonotonic, a fact which was also observed in the continuous SG case and ascribed to the interaction of the kink with internal oscillation modes [11]. On the other hand, decrease of the coupling constant makes the phase locking steps more pronounced. For $\kappa=1.5$, the dependence $\langle v \rangle (E_1)$ almost coincides with the one for $\kappa=2$ (for larger amplitudes, however, the three resonant steps $k=l=1$, $k=3,l=2$, and $k=2,l=1$ become much more visible).

Further decrease of the coupling constant makes the dependence even less monotonic: for $\kappa=1$ (shown by $\diamond$ in the figure), the nonmonotonicity is quite weak, with a small interval $0.145 < E_1 < 0.154$ in which the kink velocity drops back to zero. For $E_1 \gtrsim 0.2$, the dependence is also nonmonotonic because of the interaction of the kink with vibrational modes localized on it. For $\kappa=0.5$ and $\kappa=0.75$, the average kink velocity becomes strongly nonmonotonic function of E_1.

Notice from the right panel of Fig. 8 that several reversals of the kink motion along the E_1 axis occur. In this regard, we remark that the sign of $\langle v \rangle$ depends on the relations between ω, α, and ω_{PN}. Decrease of κ can change ω_{PN} significantly [see Eq. (4)], thus effecting the sign of the velocity. The reversals of $\langle v \rangle$ as a function of E_1, however, are not fully explained by these arguments and we believe that, in analogy with the continuous case, the coupling of the kink with small amplitude waves plays also an important role.

By comparing the left and the right panels of Fig. 8, one can also see that the nonmonotonic jumps occur in correspondence with the transitions from chaotic to regular (phase locked) regimes. In order to get a better understanding of this

behavior, we have plotted in insets (a) and (b) the mean velocity as a function of the phase difference θ. The inset (a) refers to the case $\kappa=0.75$ for two different values of the driver amplitude. We see that while for $E_1=0.19$ the dependence $\langle v \rangle (\theta)$ is piecewise, but somewhat similar to Fig. 2 (i.e., it has one minimum and one maximum), the dependence becomes more irregular as E_1 increases, with small islands of phase locked regimes with opposite velocities. A similar phenomenon is observed, when κ decreases to $\kappa=0.5$ [inset (b)]. This behavior is linked to the well known phenomenon of *crises of attractors*, i.e., to sudden appearance (or disappearance) of an attractor as a system parameter varies (see [35]). Attractor crises for one-particle ratchets have been observed in Refs. [36]. By further decreasing the coupling constant, more and more attractor crises are found.

From the insets of Fig. 8, we also see that, in contrast with the case $\kappa=1$ in Fig. 2, the dependence $\langle v \rangle = \langle v \rangle (\theta)$ loses any resemblance with a sinusoidal function for small values of κ. From Fig. 8, it is also evident that the depinning amplitude of the kink motion increases when κ decreases. For very small κ, e.g., $\kappa=0.0625$ (not shown in Fig. 8), no directed motion is found—the kink is either pinned by the lattice or destroyed by chaos when the driving amplitude becomes large enough. This behavior is not surprising, since we know that high discreteness normally prevents solitons from free propagation.

We remark that the attractor crises leading to reversal phenomena are out of the range of validity of the single particle approximation since they involve many degrees of freedom. In particular, in the limit of weak coupling, the point particle approximation (3) as well as the symmetry analysis discussed in Sec. III become not valid.

D. Internal mode mechanism and dependence on the damping parameter

In the case of continuous soliton ratchets, it was shown (see Refs. [10,11,20,21,19]) that a contribution to the ratchet phenomenon comes also from the internal oscillation of the kink via the internal mode mechanism. We expect this effect to be true also in the present case, both for large values (i.e., close to the continuum limit) and intermediate and small values of the coupling constant κ (for very small values of κ, however, the kink becomes pinned to the lattice and the ratchet phenomenon disappears as discussed above).

In the following we investigate the internal mode mechanism by fixing $\kappa=1$ and performing direct numerical simulations of Eqs. (1). In particular, we show the existence of a local oscillation on the kink profile which is, perfectly synchronized (phase locked) with the kink motion. We have found that when the dynamics of the kink center of mass is phase locked to the resonance (k,l), the internal mode oscillation is also locked to the same resonance. This is shown in Fig. 9 for the discrete kink ratchet, which is phase locked to the external driver with rotation numbers $k=2$, $l=7$. In the panel (a) of this figure, the initial and final kink profiles are depicted, from which one can conclude that these profiles perfectly coincide after $l=7$ periods of the external driver (notice that the final configuration has been shifted by two
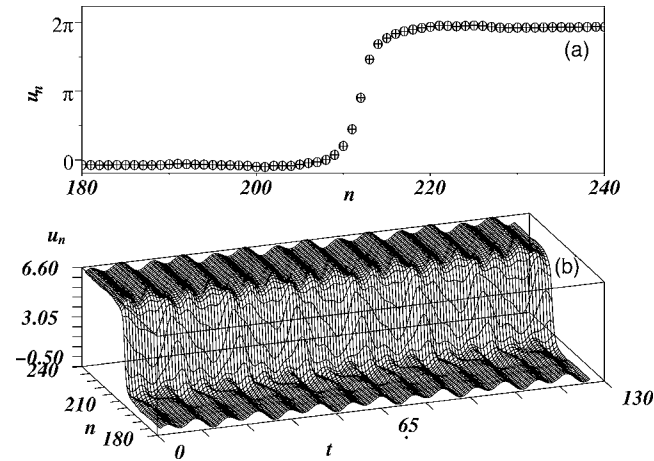
FIG. 9. Evolution of the kink profile $u_n(t)$. Upper panel shows initial kink profile (+) and kink profile after integration time $7T$ (○), shifted two sites backwards. Parameters of the model are: $E_1 = E_2 = 0.135$, $\theta = 1.5$, $\alpha = 0.1$, $\omega = 0.35$, and $\kappa = 1$.

sites backwards in order to demonstrate full coincidence).

The phase locking of the motion to the external driver is also observed from the three-dimensional plot of $u_n(t)$ in panel (b). Similar results are obtained for different values of the driving amplitudes, as one can see from Fig. 10. In this case, the kink is locked on the resonance with rotation numbers $(1,2)$ (notice that the kink reproduces itself completely after the time $2T$). In panel (b), the complete dynamics in the time interval $[0,4T]$ is also shown. The fact that the center of mass motion and the oscillations on the kink profile (internal mode) are perfectly synchronized suggests the existence of coupling between the internal and translational modes similarly as for the continuous case.

The existence of the internal mode mechanism in the discrete case is also supported by the influence of the damping
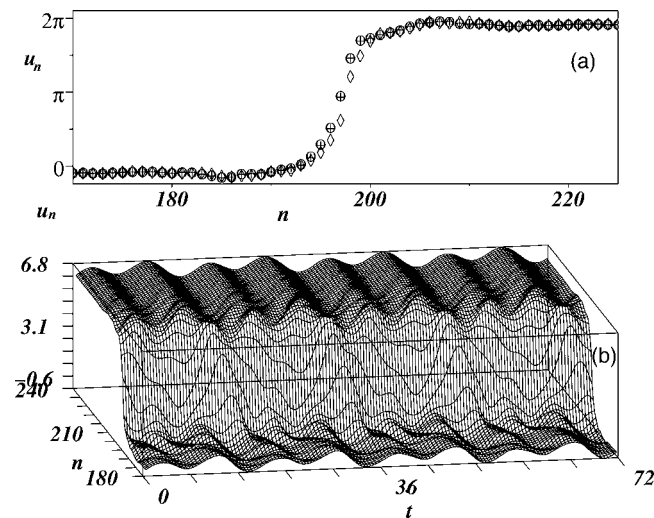

FIG. 10. Same as in Fig. 9. All parameters are the same except $E_1 = E_2 = 0.17$. In panel (a), the initial kink configuration is shown by (+), the configuration after time T (◇) and after time $2T$ (○), shifted by one site backwards. Panel (b) shows three-dimensional dynamical picture for the kink evolution in the time interval $[0,4T]$.
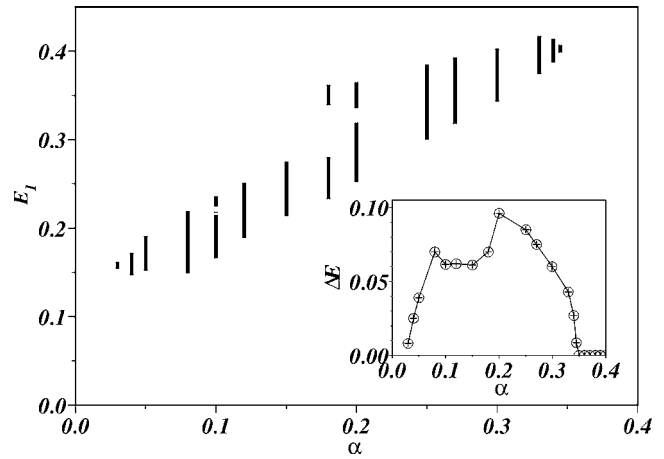

FIG. 11. Existence diagram of the main resonance ($k=l=1$) on the plane ($\alpha, E_1 = E_2$) for $\omega = 0.35$, $\theta = 2$, and $\kappa = 1$. The inset shows the dependence of the width of resonance ΔE on damping coefficient α. When the resonance consists of several islands, ΔE is computed as a sum of the widths of individual islands. The connecting line is drawn as a guide to an eye.

constant on the phenomenon. In the continuous case, it was shown that the coupling between the translational and internal modes decreases with the damping and for the case of asymmetric potentials with symmetric drivers, it was proved that in the limit $\alpha \rightarrow 0$, the coupling completely disappears [19]. In the case of biharmonic asymmetric forces, the nonlinearity induces an effective bias component, which gives rise to a point particle contribution also in the absence of damping.

The contribution of the internal mode to the ratchet dynamics, however, should be sensitive to the damping, if the coupling is controlled by the damping and the unidirectional motion should become less effective for small values of the damping constant. On the other hand, when the damping in the system becomes too large, the dynamics are strongly reduced (or stopped), so that a nonmonotonous behavior of transport with α is expected and an optimal value of the damping which maximizes the transport should exist.

In the following numerical study we have taken the width of resonance steps produced by the ratchet dynamics (see Fig. 4) as a measure of the efficiency of the transport in the system (in the experimental setting considered in Ref. [15], these resonance widths correspond to the voltage steps in the IV characteristic of a Josephson junction).

Figure 11 illustrates the width of the main resonance $(1,1)$ as a function of α (similar behavior is observed also for other resonances). It follows from this figure that the resonant steps are reduced when α is reduced and tend to disappear as $\alpha \rightarrow 0$ (for small α numerical calculations become very difficult due to longer transient times to settle on the attractor). The same behavior is observed as α increases beyond the value $\alpha \approx 0.35$. From this figure we conclude that the effect becomes maximum around an intermediate value of damping with $\alpha \approx 0.2$. The existence of an optimal coupling between the kink phase looked dynamics and its internal oscillation which maximizes the transport, indicates the validity of the internal mode mechanism also for the discrete case.
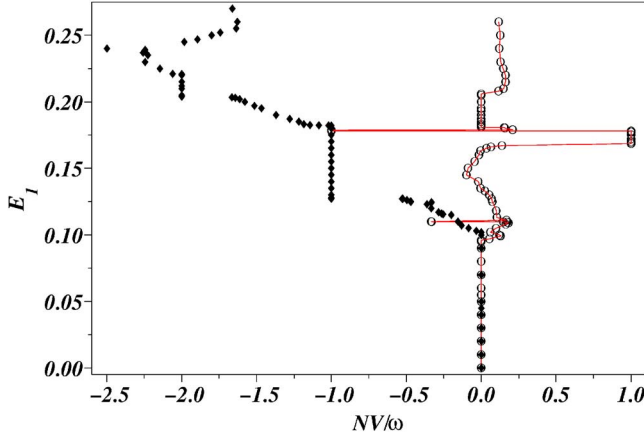
FIG. 12. (Color online) Dependence $E_1 = E_1(V)$ for $\kappa = 0.25$ ($\circ$) and $\kappa = 1$ ($\blacklozenge$). Other parameters are: $\alpha = 0.1$, $\theta = 1.5$, and $\omega = 0.35$. The array consists of $N = 10$ junctions. The connecting line for the case $\kappa = 0.25$ has been drawn as a guide for an eye.

VI. APPLICATIONS TO ARRAYS OF SMALL JOSEPHSON JUNCTIONS

In this section, we discuss possible applications of above results to the case of an array of parallel shunted and ac-biased small Josephson junctions (JJAs). This system is described by Eqs. (1) with u_n corresponding to the phase difference of the wave functions of the nth junction. The discreteness parameter equals $\kappa = \sqrt{\Phi_0/(2\pi I_c L)}$, where Φ_0 is the magnetic flux quantum, L is inductance of an elementary cell, and I_c is the critical current of an individual junction. The dimensionless dissipation parameter is then $\alpha = \Phi_0/(2\pi I_c R)$, where R is the resistance of an individual junction, and the time is normalized to the inverse Josephson plasma frequency $1/\omega_0 = \sqrt{C\Phi_0/(2\pi I_c)}$. In these systems, the topological solitary waves have the physical meaning of trapped magnetic flux quanta (fluxons) and the voltage drop V in the array is defined as

$$V = \frac{1}{N}\sum_{n=1}^{N}\lim_{t\to\infty}\frac{1}{t}\int_0^t \dot{u}_n(t')dt'. \qquad (13)$$

The experiments with annular JJAs have been performed for typical lengths $N \sim 8-30$ (see Refs. [37–39]). In the following, we consider the case of an array with $N = 10$ junctions subjected to periodic boundary conditions (annular array). From the previous analysis we expect that the ratchet dynamics of the fluxon give rise to nonzero voltage drops in the IV characteristic of the array. The voltage drop in an annular JJA (with one fluxon in it) is related to the average fluxon velocity $\langle v \rangle$ by the equation $V = 2\pi\langle v \rangle/N$ [38].

Figure 12 shows the IV characteristic of an annular JJA [dependence $E_1(V)$] for two different values of the coupling constant κ. For $\kappa = 1$ the characteristic is dominated by large phase locking steps associated to limit cycles with rotation numbers (k, l). In particular, the phase locking resonances $(k = l = 1)$ and $(k = 2, l = 1)$ are very well pronounced. On the limit cycles of this type the voltage drop is equal to $V = k\omega/(Nl)$ and for each lattice site n we have $u_n(t+lT)$
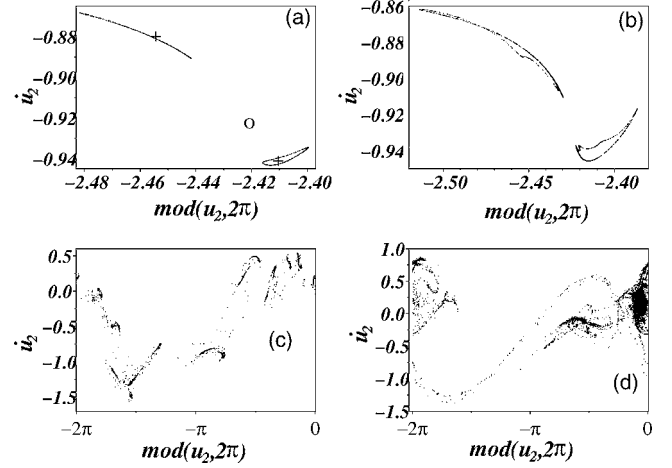

FIG. 13. Poincaré sections for $\omega = 0.35$, $\alpha = 0.1$, $\theta = 2$, and $N = 10$ and different values of driving amplitudes and coupling constants. Panels (a)–(c) correspond to case $\kappa = 1$. In panel (a), $E_1 = E_2 = 0.182$ ($\circ$), $E_1 = E_2 = 0.182\,02$ (+), $E_1 = E_2 = 0.182\,05$ (dots). In panel (b), $E_1 = E_2 = 0.182\,07$ and in panel (c), $E_1 = E_2 = 0.1821$. Panel (d) corresponds to $\kappa = 0.25$ and $E_1 = E_2 = 0.097$.

$= u_n(t) + 2\pi k$ (notice that for the phase locking dynamics, NV/ω corresponds to the ratio of the rotation numbers k/l).

For smaller values of κ (e.g., $\kappa = 0.25$) directed fluxon motion becomes diffusive almost for all values of the driving amplitudes. This behavior corresponds to the irregular (nonvertical) parts of the IV curve seen for $\kappa = 0.25$. Notice that in this case, only very few regular regimes are observed: pinning regions and very small phase locking steps with $k = \pm 1, l = 1$. An idea of complexity of the dynamics, resulting in this case, can be obtained from the Poincaré sections of one of the junctions, as reported in Fig. 13 for different values of the driver amplitudes. The Poincaré section is produced by plotting the values of the pair of the dynamical variables $\{u_n(t), \dot{u}_n(t)\}$ for $n = 2$ after the time intervals NT. The phase locking regime with the rotation numbers $k = l = 1$ is identified as the fixed point represented by the circle ($\circ$) in panel (a) of Fig. 13 and it corresponds to the fluxon which returns on the initial site (junction) after one trip around the array during the time NT. As the driving amplitude increases, the fixed point bifurcates into a period two orbit corresponding to the two crosses in the Poincaré section shown in Fig. 13(a) (the kink dynamics reproduces itself after the time $2NT$, making two trips around the array, and so on). The curves shown in panel (a) refer to the case $E_1 = E_2 = 0.182\,05$ and correspond to quasiperiodic motion. In panels (b) and (c) of Fig. 13 we report the Poincaré sections of the period-doubling route to chaos, while panel (d) shows the case with $\kappa = 0.25$ for which chaos is fully developed and the fluxon motion is strongly diffusive. A similar behavior is found for the Poincaré sections taken on other junctions in the array.

Notice the presence of voltage sign reversals in the IV characteristic in Fig. 12 generated by reversals of the direction of the motion of the kink. In particular, the sudden emergence of small intervals around $E_1 \simeq 0.178$ and $E_1 \simeq 0.11$, associated with negative voltages at the resonances $k = -1$,

$l=1$ and $k=-1, l=3$, respectively, are clearly visible. These phenomena, as discussed in the previous section, are due to attractor crises and have been observed also for other values κ as well as for longer arrays (see also Fig. 8). Comparing the dynamical behavior of arrays of different lengths (different number of junctions), we find that already for a small array of 10 junctions, the fluxon dynamics is qualitatively very similar to that obtained for the infinite chain. The quantitative difference, existing between the two cases, is probably due to the interaction of the fluxon with the radiated small amplitude waves (Josephson plasmons), this being more pronounced in the discrete case due to smaller size of the system.

VII. CONCLUSIONS

The ratchet phenomena induced by temporarily asymmetric zero mean fields on topological solitons (kinks and antikinks) of the discrete sine-Gordon equation have been investigated. In particular, we have obtained the conditions for the occurrence of discrete soliton ratchets. It has being shown that, in analogy with the continuous SG case, the unidirectional motion arises when all symmetries of the system relating orbits with opposite velocities are broken. This condition can be achieved when an external driver, consisting of the superposition of two sinusoidal signals: the main harmonic and its first overtone, satisfies suitable inequalities. In the paper the above mentioned condition has been numerically tested for different values of the relative phase between the two signals. Numerical simulations have confirmed disappearance of the directed soliton motion if the respective symmetries have been restored.

The dependence of the mean velocity of the kink on the amplitude, phase shift, and frequency of the biharmonic driver, as well as on the damping and on the coupling constant, have extensively been investigated. The main characteristic of discrete soliton ratchets, in comparison with the continuous case, is the existence of a depinning threshold (in the driver amplitude) related to the Peierls-Nabarro barrier. For driving amplitudes smaller than the critical threshold, the kink performs periodic oscillations around its center of mass,

while above this threshold, the kink directed motion takes place. Numerical studies show that the ratchet dynamics becomes pronounced when the driving frequency is smaller than all other characteristic frequencies in the system and most effective when the kink motion is phase locked to the external driver. In the phase locked regime the kink travels an integer number of sites during the integer number of the periods of the ac driver. We showed that the dependence of the velocity on the system parameters is much more complicated than in the continuous case, resembling in most cases a devil's staircase. Besides the phase locking regime we found that transport is also possible (although less effective) in the presence of chaos and intermittency. The mechanism of the kink unidirectional motion was shown to depend strongly on the coupling constant. For large and intermediate values of the coupling constant the transport is dominated by the regular phase locked trajectories while for small values of the coupling constant the diffusive chaotic nature of the kink transport dominates. Our investigation of the dependence of the kink transport on the damping constant shows that some qualitative analogy with the continuous case remains. In particular, the existence of an optimal coupling between internal and translational modes for some intermediate values of the damping strongly suggests the existence of an internal mode mechanism also in the discrete case (the dependence of the phenomenon on the internal mode requires however further investigations).

Finally, the possibility to observe experimentally discrete soliton ratchets in a one-dimensional ac-biased annular array of small Josephson junctions has been discussed in detail. From our results we predict that the kink ratchet dynamics induced by a biharmonic ac driver of zero mean leads to the formation of voltage steps in the IV characteristic of the array, in the absence of any DC bias.

[1] P. Hänggi and R. Bartussek, in: *Nonlinear Physics of Complex Systems—Current Status and Future Trends*, edited by J. Parisi, S. C. Müller, and W. Zimmermann, Lecture Notes in Physics 476, p. 294 (Springer, Berlin, 1996); F. Jülicher, A. Ajdari, and J. Prost, Rev. Mod. Phys. **69**, 1269 (1997).

[2] P. Reimann, Phys. Rep. **361**, 57 (2002).

[3] S. Flach, O. Yevtushenko, and Y. Zolotaryuk, Phys. Rev. Lett. **84**, 2358 (2000).

[4] O. Yevtushenko, S. Flach, Y. Zolotaryuk, and A. A. Ovchinnikov, Europhys. Lett. **54**, 141 (2001).

[5] S. Denisov, S. Flach, A. A. Ovchinnikov, O. Yevtushenko, and Y. Zolotaryuk, Phys. Rev. E **66**, 041104 (2002).

[6] J. L. Mateos, Phys. Rev. Lett. **84**, 258 (2000).

[7] M. Barbi and M. Salerno, Phys. Rev. E **62**, 1988 (2000).

[8] M. Barbi and M. Salerno, Phys. Rev. E **63**, 066212 (2001).

[9] F. Marchesoni, Phys. Rev. Lett. **77**, 2364 (1996).

[10] M. Salerno and N. R. Quintero, Phys. Rev. E **65**, 025602(R) (2002).

[11] M. Salerno and Y. Zolotaryuk, Phys. Rev. E **65**, 056603 (2002).

[12] S. Flach, Y. Zolotaryuk, A. E. Miroshnichenko, and M. V. Fistul, Phys. Rev. Lett. **88**, 184101 (2002).

[13] Y. Zolotaryuk, M. Salerno, and P. L. Christiansen, Int. J. Mod. Phys. B **17**, 4428 (2003).

[14] E. Goldobin, A. Sterck, and D. Koelle, Phys. Rev. E **63**, 031111 (2001).

[15] A. V. Ustinov, C. Coqui, A. Kemp, Y. Zolotaryuk, and M. Salerno, Phys. Rev. Lett. **93**, 087001 (2004).

[16] K. Seeger and W. Maurer, Solid State Commun. **27**, 603 (1978); I. Goychuk and P. Hänggi, Europhys. Lett. **43**, 503 (1998); K. N. Alekseev, E. H. Cannon, J. C. McKinney, F. V. Kusmartsev, and D. K. Campbell, Phys. Rev. Lett. **80**, 2669 (1998); K. N. Alekseev and F. V. Kusmartsev, e-print cond-mat/0012348, and references therein.

[17] G. Carapella and G. Costabile, Phys. Rev. Lett. **87**, 077002(4) (2001).

[18] M. Beck, E. Goldobin, M. Neuhaus, M. Siegel, R. Kleiner, and D. Koelle, Phys. Rev. Lett. **95**, 090603 (2005).

[19] N. R. Quintero, B. Sanchez-Rey, and M. Salerno, Phys. Rev. E **72**, 016610 (2005).

[20] L. Morales-Molina, N. R. Quintero, F. G. Mertens, and A. Sanchez, Phys. Rev. Lett. **91**, 234102 (2003).

[21] C. R. Willis and M. Farzaneh, Phys. Rev. E **69**, 056612 (2004).

[22] A. V. Savin, G. P. Tsironis, and A. V. Zolotaryuk, Phys. Rev. E **56**, 2457 (1997).

[23] L. M. Floria, F. Falo, P. J. Martínez, and J. J. Mazo, Europhys. Lett. **60**, 174 (2002).

[24] L. M. Floria, C. Baesens, and J. Gomez-Gardenes, in *Dynamics of Coupled Map Lattices and of Related Spatially Extended Systems*, edited by J.-R. Chazottes and B. Fernandez, Lecture Notes in Physics, 671, p. 209 (Springer, Berlin Heidelberg, 2005).

[25] L. M. Floria, P. J. Martínez, S. Flach, and M. V. Fistul, Physica D **187**, 100 (2004).

[26] L. M. Floria and J. J. Mazo, Adv. Phys. **45**, 505 (1996).

[27] For details on the description of the discrete kink dynamics, using the collective coordinates, see the review paper by O. M. Braun and Y. S. Kivshar, Phys. Rep. **306**, 2 (1998); and the references therein.

[28] The effect should not be confused with the soliton dynamics under the influence of a single harmonic sinusoidal signal in continuous (see Ref. [29]) or discrete (see Refs. [30–32]) media. In those cases, the soliton motion becomes dependent on the initial phase and it can occur in both directions with the same absolute value of the soliton velocity.

[29] E. Goldobin, B. A. Malomed, and A. V. Ustinov, Phys. Rev. E **65**, 056613 (2002).

[30] L. L. Bonilla and B. A. Malomed, Phys. Rev. B **43**, 11539 (1991).

[31] P. J. Martínez, F. Falo, J. J. Mazo, L. M. Floria, and A. Sanchez, Phys. Rev. B **56**, 87 (1997).

[32] G. Filatrella and B. A. Malomed, J. Phys.: Condens. Matter **11**, 7103 (1999).

[33] Y. Ishimori and T. Munakata, J. Phys. Soc. Jpn. **51**, 3367 (1982).

[34] M. Peyrard and M. D. Kruskal, Physica D **14**, 88 (1984).

[35] H. G. Schuster, *Deterministic Chaos. An Introduction* (VHC Publishers, Weinheim, 1988).

[36] J. L. Mateos, Physica D **168-169**, 205 (2002); Physica A **325**, 92 (2003).

[37] S. Watanabe, H. S. J. van der Zant, S. H. Strogatz, and T. P. Orlando, Physica D **97**, 429 (1996).

[38] A. V. Ustinov, Physica D **123**, 315 (1998).

[39] P. Binder, D. Abraimov, A. V. Ustinov, S. Flach, and Y. Zolotaryuk, Phys. Rev. Lett. **84**, 745 (2000).